

Impact of multi-messenger spectral modelling on blazar–neutrino associations

JULIAN KUHLMANN^{1,2} AND FRANCESCA CAPEL¹

¹*Max Planck Institute for Physics
Boltzmannstraße 8, 85748 Garching*

²*Technical University of Munich
James-Frank-Str. 1, 85748 Garching*

ABSTRACT

Blazars are interesting source candidates for astrophysical neutrino emission. Multi-messenger leptohadronic models based on proton–photon ($p\gamma$) interactions result in predictions for the neutrino spectra which are typically strongly peaked at high energies. In contrast, statistical analyses looking to associate blazars and neutrinos often assume a power-law spectral shape, putting the emphasis at lower energies. We aim to examine the impact of such spectral modelling assumptions on the associations of neutrinos with blazars. We use `hierarchical_nu`, a Bayesian framework for point source searches, and incorporate the theoretical predictions for neutrino spectra through a dedicated spectral model and priors on the relevant parameters. Our spectral model is based on the predictions presented in [Rodrigues et al. \(2024a\)](#) for a selection of intermediate and high synchrotron peaked blazars that have been connected with IceCube neutrino alert events. We apply our model to the 10 years of publicly available IceCube data, focusing on the Northern hemisphere. Out of 29 source candidates, we find five sources, including TXS 0506+056, that have an association probability $P_{\text{assoc}} > 0.5$ to at least one event. The $p\gamma$ spectra typically lead to a lower overall number of associated events compared to the power-law case, but retain or even enhance strong associations to high-energy events. Our results demonstrate that including more information from theoretical predictions can allow for more interpretable source–neutrino connections.

Keywords: High energy astrophysics (739) — Astronomical methods (1043) — Neutrino astronomy (1100) — Astrostatistics (1882) — Bayesian statistics (1900) — Hierarchical models (1925)

1. INTRODUCTION

Recent years have seen exciting progress in the field of neutrino astronomy. Since the first observations of energetic neutrino events ([Aartsen et al. 2013a,b](#)), the IceCube Neutrino Observatory has discovered a diffuse flux of astrophysical neutrinos ([Naab et al. 2023](#); [Alkhalverdyan et al. 2023](#)). In our neighbourhood, the Galactic plane has been shown to contribute to the diffuse neutrino flux ([Abbasi et al. 2023](#)). Furthermore, the data shows

evidence for the first transient point source, TXS 0506+056 ([Aartsen et al. 2018a,b](#)), and the first steady state point source, NGC 1068 ([Aartsen et al. 2020b](#); [Abbasi et al. 2022](#)), with hints of similar Seyfert galaxies making up the first source class ([Abbasi et al. 2024a,b](#)).

In IceCube searches using predefined source lists, two blazars other than TXS 0506+056 appear to drive incompatibility with the background hypothesis: PKS 1424+240 and GB6 J1542+6129 ([Aartsen et al. 2020a](#); [Abbasi et al. 2021](#); [Abbasi et al. 2022](#)), both belonging to the sub-class of “masquerading BL Lacs”. Despite exhibiting a nearly featureless spectrum typical of BL Lacs, mas-

quering BL Lacs have intrinsic line emission that could contribute to neutrino production (Padovani et al. 2022). In stacking searches of blazar catalogs only upper limits have been found by the IceCube collaboration (e.g. Abbasi et al. 2022a). These results are consistent with the picture of blazars as transient sources of neutrinos, but a limited contribution to the observed diffuse astrophysical flux.

Independently of the IceCube collaboration, various associations of different catalogs containing blazars and IceCube neutrinos have been found using publicly available information. For example, radio-bright AGN (Plavin et al. 2023, see also Abbasi et al. 2023a) the Roma-BZCAT (Buson et al. 2022, 2023), and intermediate- and high-synchrotron-peaked BL Lacs (Giommi et al. 2020; Giommi & Padovani 2021). The methods used to analyse public data are typically restricted to spatial correlations between individual high-energy events or “hotspots”. In these cases, the information included in the analysis is limited and therefore further physical interpretation of the results is challenging. While the angular distance is a key factor for physical associations, it is also important to consider the experimental angular resolution (also see Bellenghi et al. 2023) and event energy information to avoid spurious results. In particular, for blazars the expected neutrino emission is typically strongly peaked towards higher energies (e.g., Rodrigues et al. 2024b).

In this work, we include these aspects into our analysis and further examine the physical connection between blazars and neutrinos. We focus on the impact of using physically motivated neutrino energy spectra, leveraging the recent results from lepto-hadronic modelling of BL Lac blazars (Rodrigues et al. 2024a, hereafter R+) that have previously been proposed as physical counterparts (Giommi et al. 2020) to IceCube’s high-energy alert events (Abbasi et al. 2023b). The shape of these spectra is distinct from the power-law form typically used in point-source searches, especially at energies $\lesssim 100$ TeV. Our analysis is possible thanks to the `hierarchical_nu`¹ software (hereafter `hnu`) introduced in Capel et al. (2024). With this approach, we focus on source characteri-

sation rather than background rejection, quantifying the model and parameters which best represent the observed data. The resulting posterior distribution also allows us to evaluate the most likely energies of individual neutrino events and the corresponding neutrino–source association probability.

We describe our methods, including the model assumptions, data set and blazar source selection in Section 2. In Section 3, we first analyse the well-studied source TXS 0506+056, demonstrating our ability to reproduce previous results and quantifying the impact of the different spectral assumptions. We then extend this analysis to the sample of blazars from R+ in Section 4. Finally, we discuss our results in Section 5 and conclude in Section 6.

2. METHODS

2.1. Spectral model

We use two different spectral models for point sources: a power-law, for comparisons with results of the IceCube collaboration, and a more physical spectrum to test the predicted neutrino emission of R+.

For the power-law spectrum case, we consider

$$\frac{dN}{dE} \propto E^{-\gamma}, \quad (1)$$

where γ is the spectral index and a free parameter and E is the neutrino energy.

Going beyond this simple description, we model sources based on results of lepto-hadronic modelling and fits across the electromagnetic spectrum. For example we choose the source-averaged neutrino spectrum of Fig. A.1 in R+ (hereafter “ $p\gamma$ spectrum”) and approximate it as a flat spectrum below a break energy, E_0 , and above as a logparabola with fixed index of zero and $\beta = 0.7$,

$$\frac{dN}{dE} \propto \begin{cases} 1, & E < E_0 \\ \left(\frac{E}{E_0}\right)^{-0.7 \log(E/E_0)}, & E \geq E_0. \end{cases} \quad (2)$$

where the break energy, E_0 , is a free parameter. The parameterisation of Eq. (2) by the peak energy, E_{peak} , used in R+ can be obtained by multiplying the differential flux Eq. (2) with E^2 and finding the maximum of the resulting expression, leading to

$$E_{\text{peak}} = E_0 e^{\frac{1}{0.7}}. \quad (3)$$

¹ https://github.com/cescalara/hierarchical_nu

We display both the numerical prediction and the approximation used, Eq. (2), for some arbitrary normalisation and break energy in Fig. 1. The intrinsic error of using the source-averaged spectrum rather than the per-source prediction is on the order of 30%. This error is further surpassed by the partial insensitivity of the multi-wavelength fit to varying proton spectra, leading to different predicted neutrino spectra (R+). In this framework, these uncertainties can be accounted for in a wide prior on the peak energy.

Neutrino emission is assumed to be constant in time for both spectral models considered.

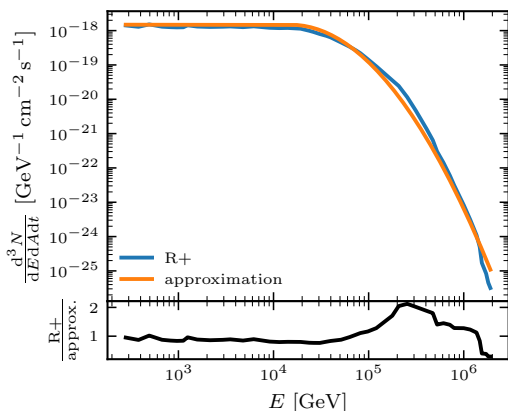


Figure 1. **Top panel:** Averaged $p\gamma$ spectrum (blue) and approximation used in this work (orange). **Bottom panel:** Ratio of $p\gamma$ and approximation.

We further model an isotropic diffuse background of astrophysical neutrinos from unresolved point sources using a power-law, Eq. (1). The atmospheric neutrino background is modelled using MCEq (Fedynitch et al. 2015), employing the hadronic interaction model SIBYLL 2.3c (Riehn et al. 2017) and the cosmic ray model H4a (Gaisser 2012). The atmospheric density profile used is NRLMSIS-00 (Picone et al. 2002) centered on the IceCube detector and averaged over a year, with the integrated flux Φ_a as sole free parameter. All source spectra are modelled between 10^2 GeV and 10^9 GeV in the detector frame. Isotropic source frame luminosities are converted to an energy flux at Earth, assuming a flat Λ CDM cosmology with $H_0 = 70 \text{ km Mpc}^{-1} \text{ s}^{-1}$, $\Omega_m = 0.7$, $\Omega_\Lambda = 0.3$. Free high-level model parameters and their prior distributions are listed in Table 1. We choose a source-dependent luminosity prior.

For each source, we calculate the luminosity which, together with an index $\gamma = 2.3$ or a source-frame peak energy $E_{\text{peak}} = 10^6$ GeV, predicts 0.1 events over the detector lifetime. This luminosity is used as μ in the lognormal prior, together with $\sigma = 4$. We have verified that results are robust against reasonable variations of this choice, e.g. using instead a luminosity corresponding to 1 expected event or $\sigma = 6$. The priors on the astrophysical diffuse spectrum reflect recent results on the differential flux normalisation ϕ_d at 100 TeV and spectral index γ_d (Naab et al. 2023).

2.2. Statistical formalism

We model emission and detection as a mixture of inhomogeneous Poisson point processes, with the mixture components reflecting the modelled source components (Streit 2010). This entails forward modelling of all source components to the data space. Further difference to the standard method, e.g. Braun et al. (2008), and implemented in SkyLLH (Wolf 2019), is that we do not marginalise over the neutrino energies but model them as latent parameters. Additionally, prior distributions of the high-level parameters are multiplied to the likelihood used. The high-dimensional, $\mathcal{O}(10^3)$, parameter space is explored by a Hamiltonian Monte Carlo algorithm implemented in the Stan programming language (Stan Development Team 2025), returning parameter samples approximating the joint posterior density. We summarise marginalised posteriors by highest posterior density regions, which are defined as the narrowest region containing α probability. In addition to posterior distributions of model parameters, we gain information on an event-by-event basis, finding posterior association probabilities of individual events to proposed point sources, P_{assoc} . For all fits we run 4 chains in parallel with 1000 warm-up samples and 4000 actual samples per chain to build the target distribution. For more details we refer to Capel et al. (2024).

As reference results of the frequentist method we find maximum likelihood estimates (MLEs) of the expected number of events \bar{n} and spectral index γ using the publicly available analysis tool SkyLLH (Kontrimas & Wolf 2021; Bellegghi et al. 2023), utilising the same public data set, see Sec. 2.3. Despite the different definitions of probability in Bayesian and frequen-

Source		Param.	Prior
	power-law	L	$\mathcal{LN}(\cdot, 4)$
		γ	$\mathcal{N}(2.3, 0.5)$
Point source	$p\gamma$	L	$\mathcal{LN}(\cdot, 4)$
		E_{peak}	$\mathcal{LN}(10^6 \text{ GeV}, 3)^{\#1}$ $\mathcal{LN}(\cdot, 0.3)^{\#2}$
Astro. diff.		ϕ_{d}	$\mathcal{N}(2.26 \times D, 0.20 \times D)$
		γ_{d}	$\mathcal{N}(2.52, 0.04)$
Atmospheric		Φ_{a}	$\mathcal{N}(0.3 \times A, 0.1 \times A)$

Table 1. Parameters and priors used throughout this work. $\mathcal{LN}(\mu, \sigma)$ and $\mathcal{N}(\mu, \sigma)$ are lognormal and normal distribution, respectively. Units of the diffuse astrophysical flux and atmospheric flux are $D = 10^{-13} \text{ GeV}^{-1} \text{ m}^{-2} \text{ s}^{-1}$ and $A = \text{m}^{-2} \text{ s}^{-1}$. Prior marked with #1 is only used in Fit #1 and defined in the source frame, and replaced by a source-dependent prior in Fit #2 (marked by #2), see Sec. 3.2 and 4 for details.

tist frameworks, parameter estimates should not be vastly different. Further, evaluating each event’s contribution to the likelihood at the MLE can be done in a frequentist analysis. The most contributing events can thus be found, but, in contrast to the Bayesian P_{assoc} , the numbers associated lack interpretability.

2.3. Data set

We apply `hnu` to 10 years of publicly available IceCube data of muon track events aimed at point source searches (IceCube Collaboration 2021). Data is selected in a region of interest (ROI) of 5° radius around the proposed point source above a reconstructed muon energy $\hat{E} = 300 \text{ GeV}$, yielding up to ~ 3700 events, depending on the source declination. We cross match events between the muon track data and IceCat-1 (Abbasi et al. 2023b) inside each ROI. Possible matches are first narrowed down by finding events with an identical arrival time to the alert event, allowing for a difference of 10^{-4} s . If more than one muon track event passes the ROI and temporal selection, we choose the highest energy muon track, which typically has an energy at least one order of magnitude larger than other muon track events with the same arrival time. These steps are needed to quantify the association of the proposed source counterparts to the alert events, as the alerts themselves are not specified in the public track data and are issued without an applicable instrument response function. The angular separation between track and alert best-fitting direction are typically $\sim 0.5^\circ$, but can be as large as $\sim 7^\circ$.

2.4. Source selection

We analyse the sources of **R+**, which have been found to be in the vicinity of IceCube alert events. We further sub-select only sources in the Northern sky above the celestial equator. Below -5° declination event rates are dominated by atmospheric muons. The formulation of the likelihood, in particular the forward modelling, necessitates knowledge of the effective area, which is not provided for muons in the employed data set (IceCube Collaboration 2021).

3. TXS 0506+056

First, we present our results for TXS 0506+056 using a power-law spectrum to show that we can reproduce the results of previous analyses and demonstrate in detail the impact of the spectral shape on our results.

3.1. Power-law

We take TXS 0506+056 as test case, using a power-law as the point source spectrum. The point source’s joint posterior density of \bar{n} and γ is shown in Fig. 2, overplotting confidence levels obtained with `SkyLLH`. Both results are in good agreement. Making use of the additional information provided by our framework we display the individual events’ association probabilities to TXS 0506+056 and energy posteriors in Fig. 3. We see that, in general, high-energy events nearby the proposed point source have a higher association probability, consistent with a point source and a hard spectral index, as indicated by the high-level posteriors.

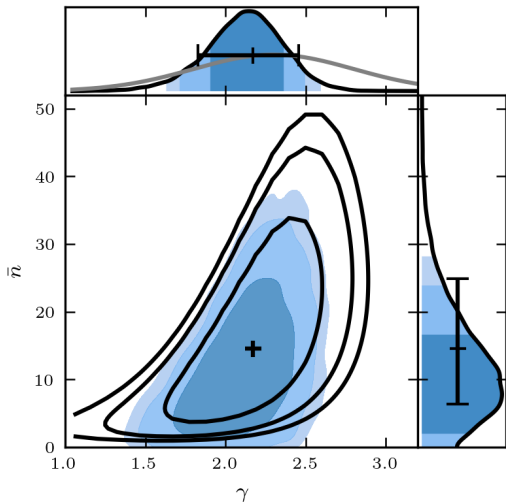


Figure 2. Joint \bar{n} and γ posterior. Filled contours show 68%, 90% and 95% credible regions from darkest to lightest. Black contours show 68%, 90% and 95% confidence levels found with `SkyLLH`. The MLE is marked by a black cross. Top and right panel show marginalised posterior densities of the same credibilities. Black errorbars show MLE and 1σ uncertainties found with `SkyLLH`.

The alert event IC170922A has $P_{\text{assoc}} = 98\%^2$. We further find an energy posterior peaked at ~ 300 TeV, in agreement with the results of [Aartsen et al. \(2018a\)](#), and a geometric mean of ~ 500 TeV (see also Fig. 5). However, there is a conceptual difference. The neutrino energy we find has been determined in the context of fitting a multi-component model to a data selection and includes all other parameters’ uncertainties, rather than determining properties of an isolated event for a given source spectrum.

3.2. $p\gamma$ spectrum

We now assume the $p\gamma$ neutrino spectrum. In a first fit we use an uninformative prior (Fit #1) on the break energy, E_0 . In a second fit, we utilise the information provided by the multi-messenger fit and place an informative prior on E_0 (Fit #2). In particular, we place a source-dependent, narrow log-normal prior on E_0 (see also Table 1) with μ corresponding to the peak

² We reported $P_{\text{assoc}} = 56\%$ for IC170922A in a single-event analysis in [Capel et al. \(2023\)](#). The smaller value can be accounted for by the use of the *deposited* energy of 23.7 TeV and circularised angular uncertainty of the alert, 0.7° ([Aartsen et al. 2018a](#)).

of the energy flux, i.e. $E_{\text{peak}} = \arg \max(\nu F_\nu)$ from Tab. E.1 in `R+`.

We compare the resulting energy fluxes against the prediction of `R+` in Fig. 4. The inferred energy flux of Fit #1, left panel, peaks at energies two to three orders of magnitude lower. Both predicted E_{peak} and the predicted flux itself are incompatible at 95% CR with our results. Compared to the frequentist parameter limits at 68% CL (dashed open contours) the allowed parameter space of Fit #1 is much more constrained due to the different definitions used to set limits on the parameters³. We now place a narrow lognormal prior informed by lepto-hadronic modelling of the multi-wavelength observations on the source frame’s break energy, accounting for redshift and conversion between E_{peak} and E_0 . The results of Fit #2 are shown in right panel of Fig. 4. Allowed fluxes are much more constrained compared to Fit #1, both in the actual flux values and the peak energy. Compared to the prediction we overestimate the flux by approximately one order of magnitude. The predicted peak, however, falls into the 68% credible region.

Comparing all three cases in Fig. 5, (power-law, $p\gamma$ with uninformative and informative priors), we find that the number of point source events decreases in that order. In particular, in the power-law case (Fig. 3) a few events at lower energies around $\dot{E} = 10^4$ GeV have intermediate association probabilities between 30% and 70%, which, in part, were detected during the 2014/15 flaring period. At even lower energies there is a larger number of fainter associations around 10%. While for both power-law fit and the uninformative $p\gamma$ fit the energy posterior of IC170922A peaks at ~ 300 TeV, for the informative $p\gamma$ fit it peaks at $\mathcal{O}(50$ PeV), driven by the informative prior. For events with intermediate P_{assoc} , the employed framework allows for an “inbetween” case with bimodal energy posteriors. In the fit to TXS 0506+056 using the $p\gamma$ model this is visible in a few events,

³ The method of [Feldman & Cousins \(1998\)](#) used in `R+` is agnostic about the realised parameters in nature. Test statistic distributions for some parameter values of E_{peak} and \bar{n} are simulated. If the simulated distributions are compatible with the test statistic found in the data analysis, the corresponding parameters of the simulations are accepted as possibly realised in nature.

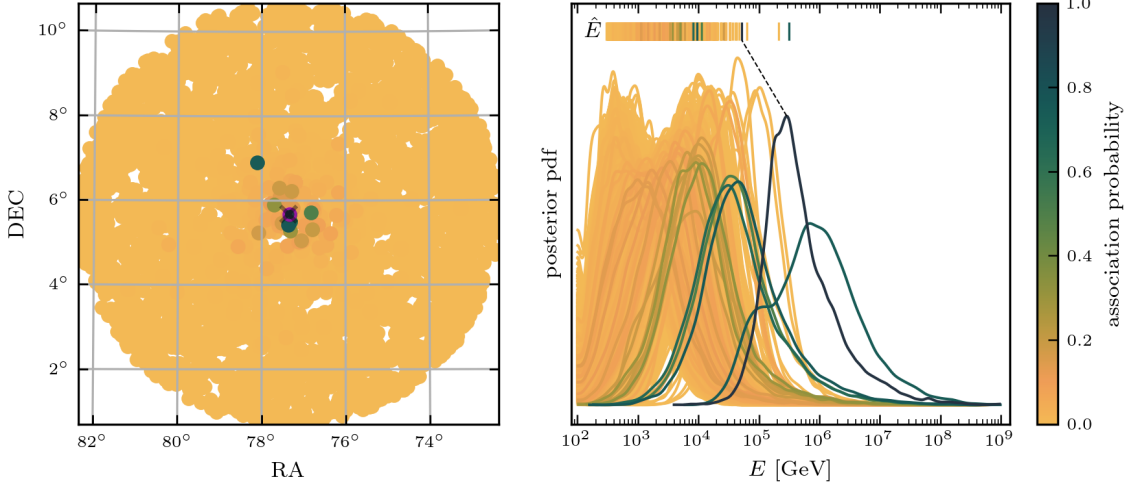


Figure 3. Analysis of TXS 0506+056 using a power-law. The colour of dots and lines reflects the posterior-averaged event association probability to TXS 0506+056. **Left panel:** Scatter plots of analysed events, projected onto the sky. The dots’ size is not connected to energy or angular uncertainty. ROI is centered on TXS, marked by a cross. The alert event IC170922A is marked by a red circle. **Right panel:** Marginalised neutrino energy posteriors of all events, transformed to $\log_{10}(E/\text{GeV})$. The upper axis shows the reconstructed muon energy of events, \hat{E} . The reconstructed energy and energy posterior of IC170922A are linked by a dashed line.

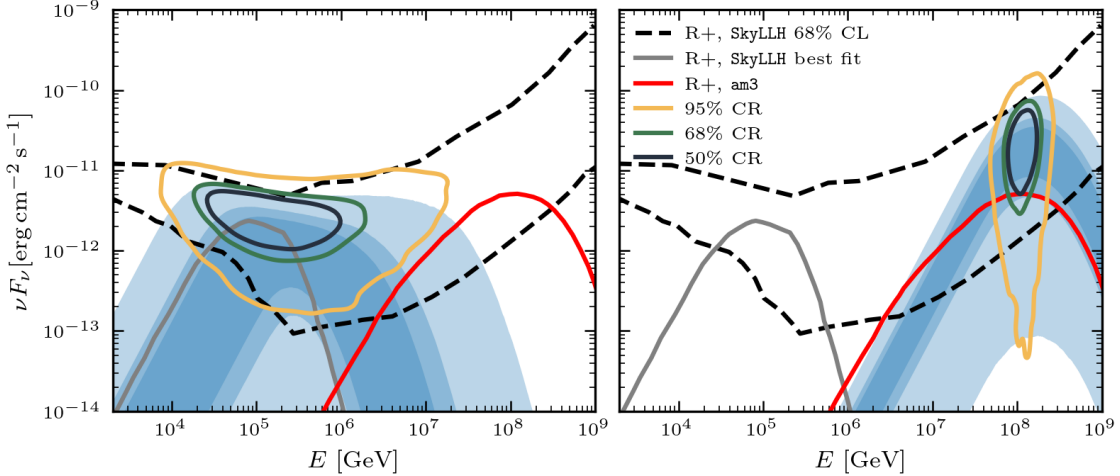


Figure 4. Analysis of TXS 0506+056 using the $p\gamma$ spectrum. Coloured bands are 50%, 68% and 95% credible regions of fluxes. Purple, green and yellow closed contours are 50%, 68% and 95% credible regions of joint posterior density of E_{peak} and peak energy flux. Grey line is best fitting neutrino flux found using SkyLLH, dashed contours are 68% CL on E_{peak} and peak energy flux. Red line is neutrino flux prediction. **Left panel:** Uninformative priors. **Right panel:** Informative E_{peak} prior. All energies are defined in the detector frame.

see second row of Fig. A1, right-most panel. Those events may either be background and have a low parent neutrino energy or belong to the point source and have an accordingly high neutrino energy. The density ratio of the posterior modes is consistent with the association probability, for $P_{\text{assoc}} > 50\%$ the mode at high

energies has a higher peak than the low energy mode.

4. BL LAC SAMPLE

For the entire selection of sources we perform three fits: using a power law, Fit #1 (uninformative prior) and Fit #2 (informative prior) using the $p\gamma$ spectrum. We show results for

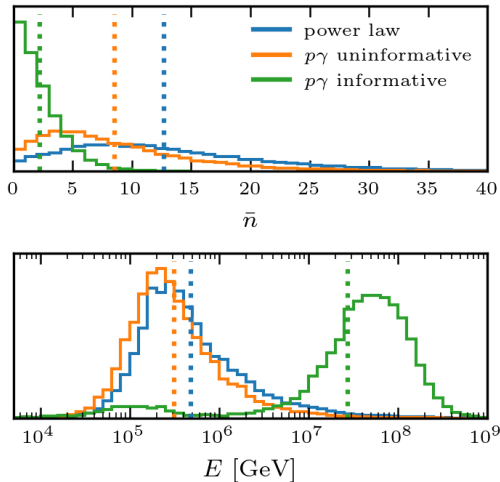


Figure 5. Comparison of fits to TXS 0506+056 with different models and priors. **Top panel:** Posterior of expected number of events. Dashed lines show the posterior means. **Bottom panel:** Energy posterior of IC170922A. Dashed lines show the geometric means of the posteriors.

the top six sources, sorted by \bar{n} in Fit #2. Figures including all sources can be found in a github repository⁴. We show for Fit #1 and #2 the inferred energy flux bands in Fig. 6, an overview of the high-level source parameters is presented in Fig. 7. For sources passing the above criteria, ROIs and energy posteriors are given in Fig. A1 in the Appendix.

The impact of the prior on the energy fluxes is clearly visible. The additional information constrains the fluxes to smaller energy ranges. In most cases the flux bands themselves also become narrower. The inferred energy fluxes tend to be higher than the predictions in Fit #2. For the sources for which we can associate neutrino emission, the inferred fluxes of Fit #2 tend to exceed the predicted peak fluxes. The associated emission would be lost if we placed a further prior on the peak energy flux. For TXS 0506+056 the added information leads to a reduction in the number of source events, as already discussed in the previous Section. In the case of 4FGL J1528.4+2004 the additional prior information on E_{peak} leads to a \bar{n} posterior less distinct from zero, $P(\bar{n} \geq 1) = 92\%$ decreases to $P(\bar{n} \geq 1) = 83\%$. We find two events at $\hat{E} = 15 \text{ TeV}, 25 \text{ TeV}$ with high association probabilities of 89% and 76% (93%

and 84% with an uninformative prior). We can not associate the proposed alert event to 4FGL J1528.4+2004. For 4FGL J2227.9+0036 we find using the uninformative prior, a substantial number of low-energy events with $P_{\text{assoc}} \geq 5\%$, leading to $\langle \bar{n} \rangle = 9.0$. All associations vanish and the \bar{n} posterior is consistent with zero when using the informative prior. We contrast the resulting event associations using a power law and Fit #2 for this source in Fig. A2.

We find a further three sources with one event exceeding $P_{\text{assoc}} = 50\%$ in either fit. In all cases this event is the corresponding alert event, see Section 4.1. For all other sources we report non-detection of emission from the proposed point sources. The \bar{n} posteriors are consistent with zero and the added information on E_{peak} helps to constrain source luminosities further, with their posteriors shrinking accordingly. In general, the posterior-averaged \bar{n} is highest for power laws and further decreases for the informative E_{peak} prior, see Tab. 2.

4.1. Connection to alert events

We can link four sources to their respective alert events above $P_{\text{assoc}} = 50\%$ in either fit. IC170922A is linked to TXS 0506+056 at 92% (98%) probability in Fit #2 (Fit #1). For 4FGL J0854.0+2753's alert (IC150904A) we find $P_{\text{assoc}} = 96\%$ (93%). The \bar{n} posterior, while consistent with zero, has a substantial tail to higher values unaffected by the prior choice. 4FGL J0158.8+0101 is linked to its alert event (Diffuse (II.1)⁵) at $P_{\text{assoc}} = 81\%$ (69%).

For the alert event IC110610A two possible counterparts have been proposed, a masquerading BL Lac, 4FGL J1808.2+3500, and a true BL Lac, 4FGL J1808.8+3522. The latter source displays the higher P_{assoc} at 56% (58%), while the former only reaches 22% in Fit #2.

4FGL 0244.7+1316 can be linked to its alert (IC161103A) at 24% in Fit #2.

For all other sources P_{assoc} of the associated alert event is consistent with zero, notably also for 4FGL 1528.4+2004 (Diffuse (II.10)), despite showing evidence for neutrino emission. For completeness, we list P_{assoc} of the alert

⁴ To be made accessible by the time of publication.

⁵ See Abbasi et al. (2022b, Table 8)

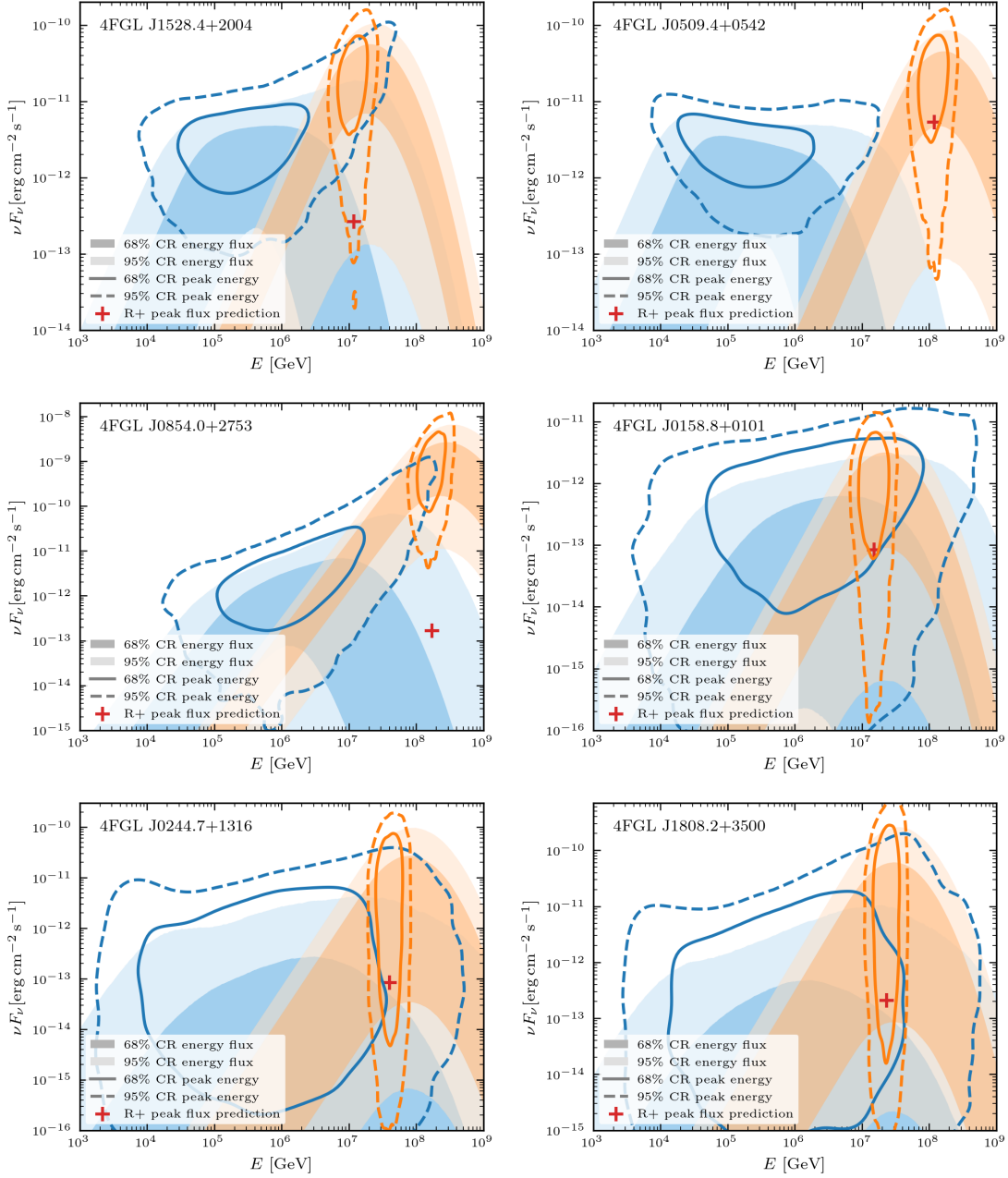


Figure 6. Point source energy fluxes. Filled bands show the 68% and 95% CR of energy flux using an uninformative prior on the peak energy E_{peak} (blue) and an informative prior (orange). Solid and dashed lines show the 68% and 95% CR of the joint peak energy and peak energy flux posterior.

events and event with the highest P_{assoc} for all sources in Table 2.

We also show our results for the total blazar sample in terms of upper limits and 68% CR on their possible contribution to the diffuse flux from the fit to this data set in Figure 8. Due to the a priori source selection above the celestial equator we normalise the flux by 2π for the differential sr^{-1} .

5. DISCUSSION

Using a power-law spectral model, we are able to confirm previous results of the IceCube collaboration for TXS 0506+056 (Aartsen et al. 2018a,b). High-level parameters agree between this work and the standard frequentist approach. Additionally, we gain insight on an event-by-event basis by modelling neutrino energies as latent parameters and reproduce the neutrino energy of IC170922A of

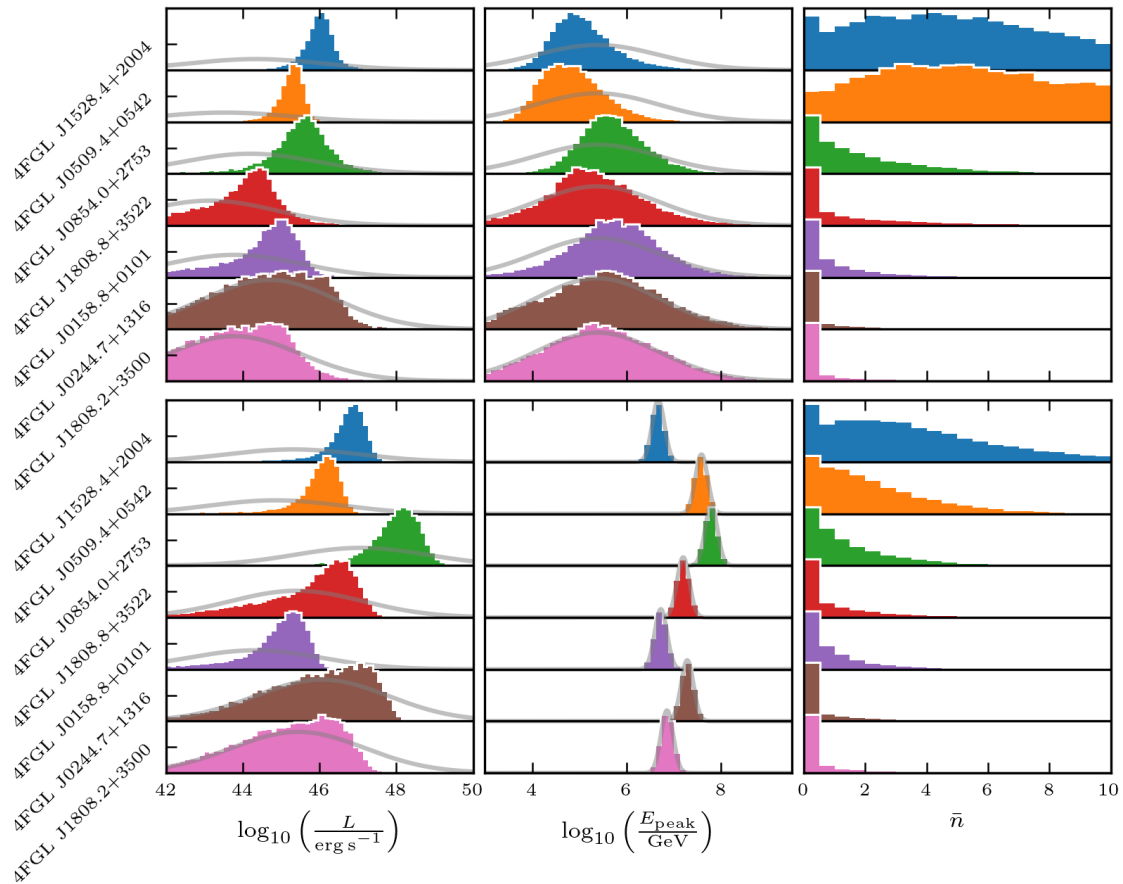


Figure 7. Marginalised posteriors of high-level point source parameters. Top (bottom) panels show posteriors obtained with the uninformative (informative) E_{peak} prior. Prior distributions are shown in grey, where applicable. E_{peak} is defined in the source frame.

$\mathcal{O}(300 \text{ TeV})$ under the assumption of a power-law, but with a spectral model informed by the entire selection of data. Utilising a spectral model typical of $p\gamma$ interactions in blazar jets and informed by multi-messenger observations, neutrino energies are expected to exceed 10 PeV. Additional prior information on E_{peak} helps to constrain the luminosities and number of expected events, apparent in more concentrated posterior distributions. Events detected during the 2014/15 flaring period with intermediate P_{assoc} become part of the background due to the informative prior, hinting at a strong dependence on the spectral model. Our prior input is based on models to time-averaged multi-wavelength observations, while TXS 0506+056 exhibits flaring behaviour (Aartsen et al. 2018a). Neutrino emission in 2014/15 also takes place at lower energies (Aartsen et al. 2018b). Reconciling these observations would necessitate time-resolved

modelling of the different flares and quiescent states. While this is beyond the scope of this work, we will explore this direction in future work. We find for most sources without evidence for neutrino emissions peak neutrino energy fluxes that are compatible with the predictions of R+, in Fit #1 typically only at 95% CR and in Fit #2 at 68% CR. The \bar{n} posteriors tend to shrink because of the informative priors. Furthermore, we find stronger constraints on the source luminosities.

The association of many low-energy events at levels of $\sim 10\%$ is suppressed by employing the $p\gamma$ model, and further vanishes in most cases by the use of the informative prior. Falling power-laws are concentrated at lower energies, whereas the $p\gamma$ spectrum is a flat power-law ($\gamma = 0$) up to the break energy. Events with high \hat{E} are then driving the position of the E_{peak} . Due to this constraint the association of lower-energy events to the point source is

4FGL	Alert event P_{assoc}			max P_{assoc} event			$\langle \bar{n} \rangle$			Pr($\bar{n} \geq 1$)		
	PL	Fit #1	Fit #2	PL	Fit #1	Fit #2	PL	Fit #1	Fit #2	PL	Fit #1	Fit #2
J1528.4+2004	0.00	0.00	0.00	0.87	0.93	0.89	8.6	6.6	3.8	0.88	0.92	0.83
J0509.4+0542*	0.98	0.98	0.92	0.98	0.98	0.92	12.7	8.5	2.2	0.98	0.95	0.69
J0854.0+2753*	0.80	0.93	0.96	0.80	0.93	0.96	3.7	2.0	1.5	0.64	0.59	0.51
J1808.8+3522*	0.43	0.58	0.56	0.43	0.58	0.56	3.9	2.1	1.1	0.47	0.44	0.35
J0158.8+0101*	0.54	0.69	0.81	0.54	0.69	0.81	1.5	1.1	0.9	0.36	0.34	0.33
J0244.7+1316*	0.08	0.14	0.24	0.08	0.14	0.24	1.1	0.7	0.7	0.20	0.18	0.20
J1808.2+3500*	0.11	0.19	0.22	0.11	0.19	0.22	1.4	0.8	0.5	0.22	0.19	0.16
J2133.1+2529	0.00	0.00	0.00	0.17	0.24	0.04	5.0	6.1	0.5	0.40	0.41	0.11
J1258.4+2123 [‡]	0.00	0.00	0.00	0.05	0.09	0.12	0.9	0.6	0.4	0.17	0.14	0.13
J2223.3+0102	0.00	0.00	0.00	0.13	0.17	0.12	1.3	1.0	0.4	0.23	0.22	0.13
J2030.5+2235	0.00	0.00	0.00	0.16	0.17	0.08	1.9	1.4	0.4	0.26	0.22	0.12
J0224.2+1616	0.01	0.02	0.04	0.12	0.12	0.04	1.5	1.1	0.4	0.23	0.19	0.11
J2030.9+1935	0.00	0.00	0.00	0.05	0.05	0.05	1.3	1.0	0.3	0.20	0.16	0.10
J1124.0+2045	0.00	0.00	0.00	0.08	0.07	0.03	1.6	0.9	0.3	0.22	0.15	0.09
J1117.0+2013	0.00	0.00	0.00	0.02	0.01	0.02	0.5	0.4	0.3	0.12	0.09	0.08
J2326.2+0113	0.00	0.00	0.00	0.22	0.27	0.11	1.4	1.0	0.3	0.25	0.22	0.09
J1300.0+1753	0.00	0.00	0.00	0.04	0.03	0.03	0.9	0.5	0.3	0.16	0.12	0.08
J1554.2+2008	0.01	0.01	0.02	0.04	0.03	0.02	0.6	0.4	0.2	0.13	0.10	0.07
J1314.7+2348	0.00	0.00	0.00	0.02	0.02	0.02	0.4	0.3	0.2	0.11	0.08	0.06
J0955.1+3551 [†]	–	–	–	0.03	0.02	0.02	0.7	0.4	0.2	0.15	0.08	0.06
J1124.9+2143	0.00	0.00	0.00	0.01	0.02	0.02	0.4	0.3	0.2	0.10	0.08	0.06
J1533.2+1855	0.00	0.00	0.00	0.04	0.06	0.01	0.7	1.2	0.2	0.14	0.30	0.06
J2227.9+0036	0.00	0.00	0.00	0.34	0.47	0.03	7.4	9.0	0.2	0.54	0.64	0.06
J0239.5+1326	0.00	0.00	0.00	0.01	0.02	0.03	0.3	0.3	0.2	0.08	0.07	0.06
J1321.9+3219	0.00	0.00	0.00	0.03	0.02	0.01	0.5	0.7	0.2	0.12	0.17	0.05
J0946.2+0104 [†]	–	–	–	0.01	0.02	0.01	0.4	0.3	0.2	0.10	0.07	0.04
J0232.8+2018	0.00	0.00	0.00	0.03	0.02	0.01	0.7	0.5	0.2	0.14	0.10	0.04
J0344.4+3432	0.00	0.00	0.00	0.01	0.01	0.00	0.3	0.2	0.2	0.09	0.05	0.04
J1003.4+0205 [†]	–	–	–	0.01	0.01	0.00	0.3	0.2	0.1	0.08	0.05	0.03

Table 2. Association probabilities of alert event (columns 2 to 4) and event with the highest source association (columns 5 to 7), posterior-averaged number of expected events, $\langle \bar{n} \rangle$ (columns 8 to 10), and probability of $\bar{n} \geq 1$ (columns 11 to 13), for all three performed fits (power law, $p\gamma$ with uninformative prior and $p\gamma$ with informative prior). For the sources marked with an asterisk the alert event scores highest in all fits. For the sources marked with a dagger the associated alert event lies outside the time range covered by the public track data. Source marked by a ‡ appears only in the 3FGL catalog.

relatively suppressed. Forcing E_{peak} to be at high energies via an informative prior centered on PeV energies, there is even less chance of observing events of a point source at low (reconstructed) energies and thus events with a previously low P_{assoc} are now firmly part of the background. In the case of TXS 0506+056, the number of events with $P_{\text{assoc}} \geq 5\%$ decreases from 39 to 26 and 5 going from the power-law model to the uninformed $p\gamma$ and finally the informed $p\gamma$ fit. Accordingly, the energy posteriors of events with considerable association probability are concentrated at very high energies, $E \gtrsim 10$ PeV, e.g. Fig. 5. Compared to the ~ 300 TeV found in the power-law analysis of IC170922A, this is a drastic change in parent neutrino energy. While this, naively, makes a detection more difficult, the association of low-energy events appears unphysical in the first place given the proposed neutrino emission mechanism.

Out of the other sources considered here, the most intriguing are 4FGL J0158.8+0101, 4FGL J0854.0+2753 and 4FGL J1528.4+2004. The former two because of the posterior association to its alert event at $P_{\text{assoc}} \gtrsim 80\%$, and the latter because of the refuted link to an alert event, and yet showing some evidence of neutrino emission. We find two events associated to 4FGL J1528.4+2004 at $\sim 80 \dots 90\%$. The similarity of the source’s posteriors to those of TXS 0506+056 make it a prime candidate for further study. In the case of alert event IC110610A both proposed sources show a tentative association, although neither is large enough to claim a discovery.

It has been argued that masquerading BL Lacs, due to their line emission acting as a target for proton-gamma collisions, are a promising source class of high-energy neutrinos, e.g. Padovani et al. (2022). Of the sources analysed in this work show-

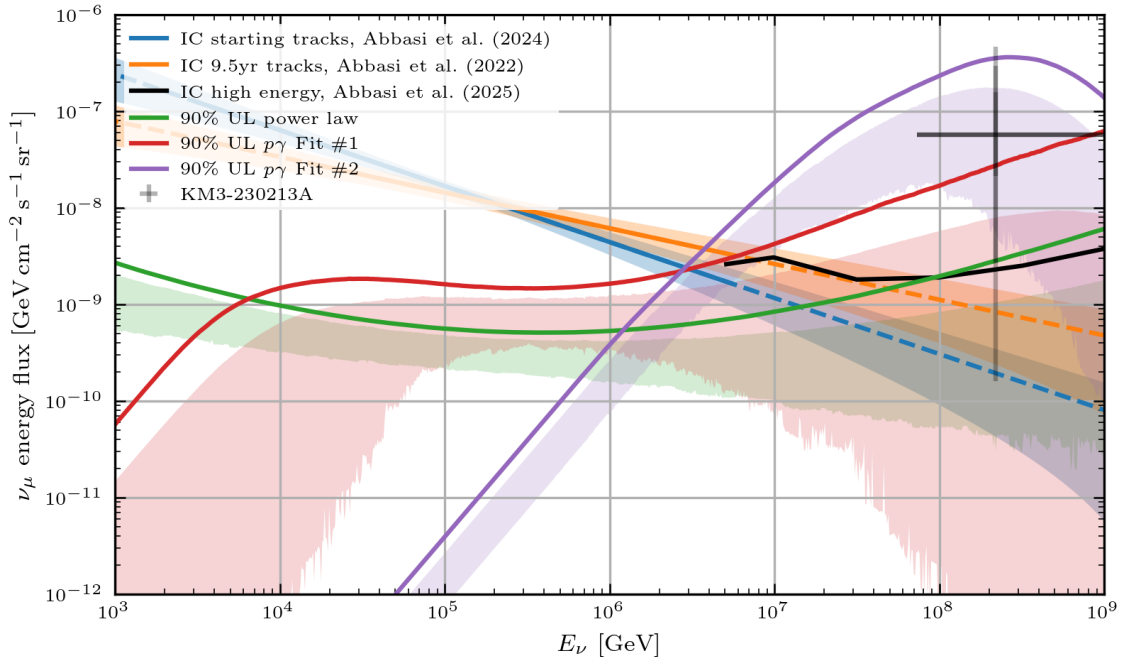


Figure 8. The contribution to the diffuse flux of the 29 blazars considered here. Filled bands are 68% CL (blue and orange)/CR (green, red, and purple), respectively. Single data point shows flux of [KM3Net Collaboration et al. \(2025a\)](#) with 1, 2, and 3σ energy flux uncertainties.

ing evidence for neutrino emission or at least exhibiting a low association to an alert event, we find four masquerading BL Lacs, 4FGL J0509.4+0542 (TXS 0506+056), 4FGL J1528.4+2004, 4FGL J0158.8+0101 and 4FGL J1808.2+3500, and two true BL Lacs, 4FGL J0854.0+2753 4FGL J1808.8+3522. The latter sources of both lists are linked to the same alert event.

The best-fitting direction of an alert event and its corresponding event of the 10 year track data typically moves on the order of 0.5° . In case of 4FGL J1321.9+3219/IC120515A the separation is approximately 5° and in the most extreme case found in the IceCat-1 catalog $\sim 7^\circ$. Additionally, the angular uncertainties are considerably smaller for the corresponding muon tracks in most cases, see Fig. A1 in the Appendix. In the case of IC110610A, both proposed counterparts, 4FGL J1808.8+3522 and 4FGL J1808.2+3500, lie approximately on the 90% containment radius of the track’s angular uncertainty, and are well within the alert event’s 90% bounding box. Even small unaccounted for effects are likely to have drastic impacts on the results. More information is needed in those cases to determine the link between alert event and possible source counter-

part. For example, systematic uncertainties in reconstruction of the arrival direction could be included in this framework by one or more additional latent parameters if such information was available. Further solidifying or disproving links between (alert) events and source counterparts can be achieved by inclusion of temporal information, which is planned as a future extension of the `hnu` framework.

6. CONCLUSIONS

We have analysed a sample of 29 BL Lacs in the Northern hemisphere taken from `R+`, searching for possible neutrino emission. In addition to the often-used power-law model for the energy spectrum, we also implemented a $p\gamma$ spectrum based on the expected neutrino emission resulting from interactions between matter and radiation fields present in blazar jets. Our results show that the choice of energy spectrum has a strong impact on both the association probability of individual high-energy neutrino alerts and the overall number of neutrinos that can be connected to the blazars in our sample.

When including an informative prior on the $p\gamma$ spectrum from theoretical predictions, we see that possible associations with individual energetic neutrinos requires their true energy to be $\gtrsim 10$ PeV, roughly two orders of mag-

nitude higher than that found with a power-law assumption. Furthermore, associations with lower-energy events that are permitted by power-law fits are no longer viable. We compare the goodness-of-fit between the power-law and $p\gamma$ cases using posterior predictive checks and find that both models give a reasonable fit to the data with no significant preference for one model over the other.

The currently limited public information on IceCube’s detector response and possible systematics could have an impact on the results reported here. While the energy resolution for through-going track events used here is naturally limited due to the unknown location of the interaction point of the neutrino, the coarse binning of the public energy resolution (in both neutrino energies and declination) exaggerates this effect, making it harder to distinguish possible parent neutrino energies. Furthermore, the event–source association strongly depends on the angular separation and angular resolution used. We note that there can be significant differences in the best-fit direction reported for the alert events and the corresponding cross-matched event in the public track dataset. In extreme cases, this systematic shift can be larger than the reported reconstruction uncertainty. Additionally, the Rayleigh distribution used to describe the angular resolution may not be the best description of the reconstructed event direction and has been updated in the latest IceCube analyses (e.g. [Abasi et al. 2022](#)). However, we do not expect these considerations to impact the overall conclusions of our work regarding the importance of spectral modelling in determining source–neutrino associations.

Considering the physically-motivated and informative $p\gamma$ model, we find four promising blazar source candidates (in addition to TXS 0506+056) that still show a strong connection to neutrino events in this more constraining framework: 4FGL J1528.4+2004, 4FGL J0854.0+2753, 4FGL J1808.8+3522 and 4FGL J0158.8+0101. Two of these sources are masquerading Bl Lacs and two are true BL Lacs. These sources have $P_{\text{assoc}} > 0.5$ to individual energetic events and an expected number of neutrino events of $\bar{n} \gtrsim 1$. Given that blazars are highly variable sources, further analysis making use of time-dependent spectral modelling will be necessary to determine if

these associations make physical sense. While this is challenging due to the availability of simultaneous observations across multiple wavelengths, we plan to investigate this direction in future work.

We further see the impact of the power-law and $p\gamma$ spectral assumptions in our results for the constraints on the diffuse flux from all the blazars in our sample. As expected, the $p\gamma$ spectrum leads to a much larger contribution in the 10–100 PeV range while still being consistent with the public IceCube tracks data set considered here. These results are particularly interesting in light of the recent detection of a ~ 100 PeV neutrino event by KM3Net ([KM3NeT Collaboration et al. 2025a](#)). While there are several blazars consistent with the uncertainty region, thus far there is no conclusive evidence for an association ([KM3NeT Collaboration et al. 2025b](#)), and it remains unclear whether this event is of cosmogenic origin.

Our results demonstrate the importance of physical spectral modelling for source–neutrino associations. In future, we plan to include complementary data sets with improved energy resolution (e.g. cascades, starting events) and time-dependent information into our analyses to improve the constraining power and further enable the interpretable connection of neutrinos with candidate sources.

- 1 The authors express their thanks to Xavier Rodrigues and Martina Karl for discussion, and to
- 2 Cristina Lagunas Gualda for discussions about
- 3 IceCube’s alert events and feedback on the
- 4 draft. The authors further acknowledge Thara
- 5 Caba for crossmatching alert events with the
- 6 public track data, and Jarred Green for provid-
- 7 ing the colour map used in this work. J.K. ac-
- 8 knowledges support from the DFG through
- 9 the Sonderforschungsbereich SFB 1258 “Neu-
- 10 trinos and Dark Matter in Astro- and Particle
- 11 Physics” (NDM).
- 12

Facilities: Computations were performed on the HPC systems Raven and Viper at the Max Planck Computing and Data Facility. This research has made use of the SIMBAD database, operated at CDS, Strasbourg, France [Wenger et al. \(2000\)](#).

Software: `arviz` (Kumar et al. 2019), `astropy` (Astropy Collaboration et al. 2013, 2018), `h5py` (Collette 2013; Collette et al. 2023), `matplotlib` (Hunter 2007), `numpy` (Harris et al. 2020), `scipy` (Virtanen et al. 2020), `seaborn` (Waskom 2021), `stan` and `cmdstanpy` (Stan Development Team 2025).

APPENDIX

A. RESULT PLOTS

REFERENCES

- Aartsen, M., Ackermann, M., Adams, J., et al. 2020a, *Physical Review Letters*, 124, doi: [10.1103/physrevlett.124.051103](https://doi.org/10.1103/physrevlett.124.051103)
- Aartsen, M. G., Abbasi, R., Abdou, Y., et al. 2013a, *Physical Review Letters*, 111, doi: [10.1103/physrevlett.111.021103](https://doi.org/10.1103/physrevlett.111.021103)
- . 2013b, *Science*, 342, doi: [10.1126/science.1242856](https://doi.org/10.1126/science.1242856)
- Aartsen, M. G., Ackermann, M., Adams, J., et al. 2018a, *Science*, 361, eaat1378, doi: [10.1126/science.aat1378](https://doi.org/10.1126/science.aat1378)
- . 2018b, *Science*, 361, 147, doi: [10.1126/science.aat2890](https://doi.org/10.1126/science.aat2890)
- Aartsen, M. G., Ackermann, M., Adams, J., et al. 2020b, *Physical Review Letters*, 124, 051103, doi: [10.1103/physrevlett.124.051103](https://doi.org/10.1103/physrevlett.124.051103)
- Abbasi, R., Ackermann, M., Adams, J., et al. 2021, *ApJL*, 920, L45, doi: [10.3847/2041-8213/ac2c7b](https://doi.org/10.3847/2041-8213/ac2c7b)
- Abbasi, R., Ackermann, M., Adams, J., et al. 2022, *Science*, 378, 538, doi: [10.1126/science.abg3395](https://doi.org/10.1126/science.abg3395)
- Abbasi, R., Ackermann, M., Adams, J., et al. 2022a, *ApJ*, 938, 38, doi: [10.3847/1538-4357/ac8de4](https://doi.org/10.3847/1538-4357/ac8de4)
- . 2022b, *ApJ*, 928, 50, doi: [10.3847/1538-4357/ac4d29](https://doi.org/10.3847/1538-4357/ac4d29)
- Abbasi, R., Ackermann, M., Adams, J., et al. 2023, *Science*, 380, 1338, doi: [10.1126/science.adc9818](https://doi.org/10.1126/science.adc9818)
- Abbasi, R., Ackermann, M., Adams, J., et al. 2023a, *ApJ*, 954, 75, doi: [10.3847/1538-4357/acdfcb](https://doi.org/10.3847/1538-4357/acdfcb)
- . 2023b, *ApJS*, 269, 25, doi: [10.3847/1538-4365/acfa95](https://doi.org/10.3847/1538-4365/acfa95)
- Abbasi, R., Ackermann, M., Adams, J., et al. 2024a, IceCube Search for Neutrino Emission from X-ray Bright Seyfert Galaxies. <https://arxiv.org/abs/2406.07601>
- . 2024b, Search for neutrino emission from hard X-ray AGN with IceCube. <https://arxiv.org/abs/2406.06684>
- Allakhverdyan, V. A., Avrorin, A. D., Avrorin, A. V., et al. 2023, *Phys. Rev. D*, 107, 042005, doi: [10.1103/PhysRevD.107.042005](https://doi.org/10.1103/PhysRevD.107.042005)
- Astropy Collaboration, Robitaille, T. P., Tollerud, E. J., et al. 2013, *A&A*, 558, A33, doi: [10.1051/0004-6361/201322068](https://doi.org/10.1051/0004-6361/201322068)
- Astropy Collaboration, Price-Whelan, A. M., Sipőcz, B. M., et al. 2018, *AJ*, 156, 123, doi: [10.3847/1538-3881/aabc4f](https://doi.org/10.3847/1538-3881/aabc4f)
- Bellenghi, C., Karl, M., & Wolf, M. 2023, Extending SkyLLH software for neutrino point source analyses with 10 years of IceCube public data. <https://arxiv.org/abs/2308.12733>
- Bellenghi, C., Padovani, P., Resconi, E., & Giommi, P. 2023, *ApJL*, 955, L32, doi: [10.3847/2041-8213/acf711](https://doi.org/10.3847/2041-8213/acf711)
- Braun, J., Dumm, J., Palma, F. D., et al. 2008, *Astroparticle Physics*, 299, doi: [10.1016/j.astropartphys.2008.02.007](https://doi.org/10.1016/j.astropartphys.2008.02.007)
- Buson, S., Tramacere, A., Pfeiffer, L., et al. 2022, *The Astrophysical Journal Letters*, 933, L43, doi: [10.3847/2041-8213/ac7d5b](https://doi.org/10.3847/2041-8213/ac7d5b)
- Buson, S., Tramacere, A., Oswald, L., et al. 2023, Extragalactic neutrino factories. <https://arxiv.org/abs/2305.11263>
- Capel, F., Kuhlmann, J., Haack, C., et al. 2023, in *Proceedings of 38th International Cosmic Ray Conference — PoS(ICRC2023)*, Vol. 444, 1576, doi: [10.22323/1.444.1576](https://doi.org/10.22323/1.444.1576)
- Capel, F., Kuhlmann, J., Haack, C., et al. 2024, *The Astrophysical Journal*, 976, 127, doi: [10.3847/1538-4357/ad7fe9](https://doi.org/10.3847/1538-4357/ad7fe9)
- Collette, A. 2013, *Python and HDF5* (O'Reilly)
- Collette, A., Kluyver, T., Caswell, T. A., et al. 2023, doi: [10.5281/zenodo.7560547](https://doi.org/10.5281/zenodo.7560547)

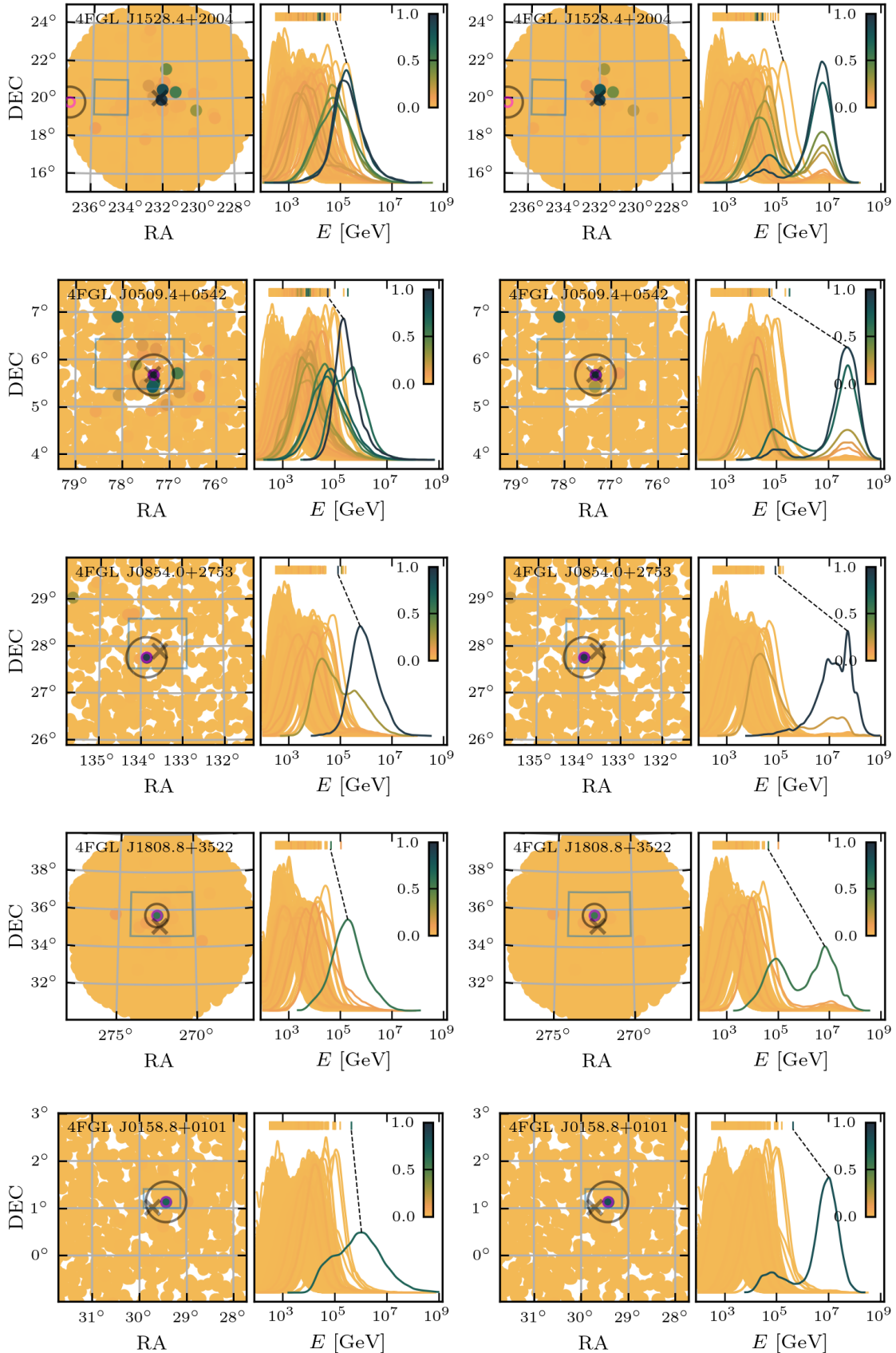


Figure A1. Event-wise analyses of fits. Left (right) column shows results using an uninformative (informative) E_0 prior. Position of alert events included in [IceCube Collaboration \(2021\)](#) are marked by a magenta circle, their 90% angular uncertainty is shown as a grey circle. A box enclosing the 90% likelihood contour of associated IceCat-1 events is plotted in light blue. The alert events' reconstructed energy is linked to their respective energy posterior by a dashed line.

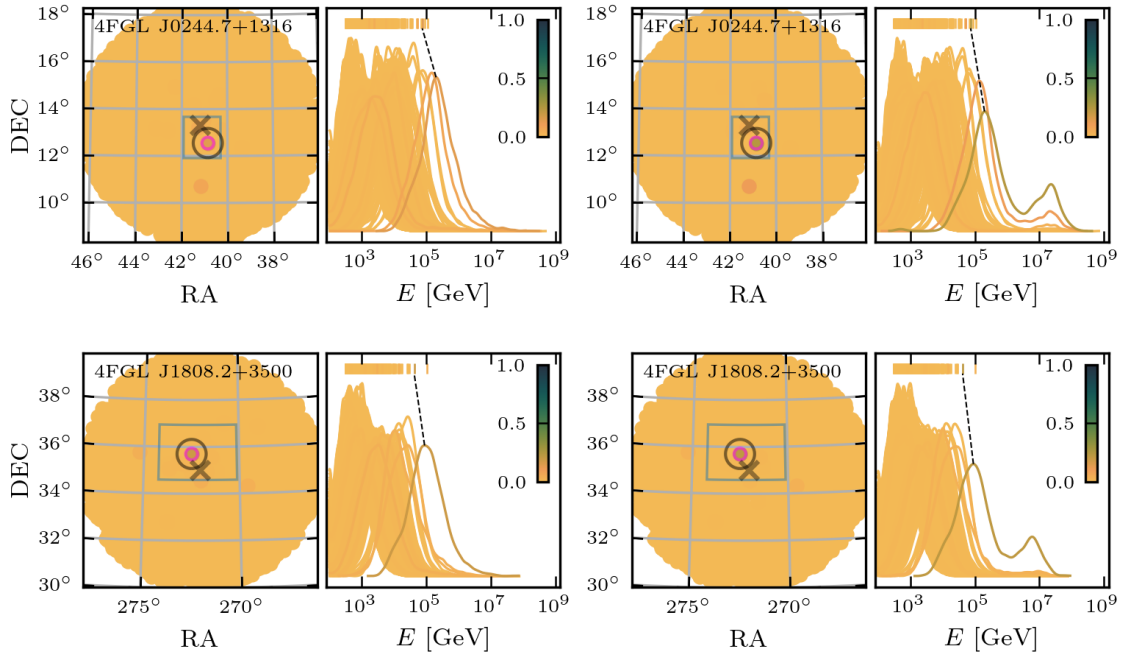


Figure A1 (Cont.).

- Fedynitch, A., Engel, R., Gaisser, T. K., Riehn, F., & Stanev, T. 2015, Calculation of conventional and prompt lepton fluxes at very high energy. <https://arxiv.org/abs/1503.00544>
- Feldman, G. J., & Cousins, R. D. 1998, Phys. Rev. D, 57, 3873, doi: [10.1103/PhysRevD.57.3873](https://doi.org/10.1103/PhysRevD.57.3873)
- Gaisser, T. K. 2012, Astroparticle Physics, 35, 801, doi: [10.1016/j.astropartphys.2012.02.010](https://doi.org/10.1016/j.astropartphys.2012.02.010)
- Giommi, P., Glauch, T., Padovani, P., et al. 2020, Monthly Notices of the Royal Astronomical Society, 497, 865–878, doi: [10.1093/mnras/staa2082](https://doi.org/10.1093/mnras/staa2082)
- Giommi, P., & Padovani, P. 2021, Universe, 7, 492, doi: [10.3390/universe7120492](https://doi.org/10.3390/universe7120492)
- Harris, C. R., Millman, K. J., van der Walt, S. J., et al. 2020, Nature, 585, 357, doi: [10.1038/s41586-020-2649-2](https://doi.org/10.1038/s41586-020-2649-2)
- Hunter, J. D. 2007, Computing in Science & Engineering, 9, 90, doi: [10.1109/MCSE.2007.55](https://doi.org/10.1109/MCSE.2007.55)
- IceCube Collaboration. 2021, IceCube Data for Neutrino Point-Source Searches Years 2008–2018, IceCube Neutrino Observatory, doi: [10.21234/CPKQ-K003](https://doi.org/10.21234/CPKQ-K003)
- KM3NeT Collaboration, Aiello, S., Albert, A., et al. 2025a, Nature, 638, 376, doi: [10.1038/s41586-024-08543-1](https://doi.org/10.1038/s41586-024-08543-1)
- KM3NeT Collaboration, MessMapp Group, LAT Collaboration, et al. 2025b, Characterising Candidate Blazar Counterparts of the Ultra-High-Energy Event KM3-230213A. <https://arxiv.org/abs/2502.08484>
- Kontrimas, T., & Wolf, M. 2021, in Proceedings of 37th International Cosmic Ray Conference — PoS(ICRC2021), Vol. 395, 1073, doi: [10.22323/1.395.1073](https://doi.org/10.22323/1.395.1073)
- Kumar, R., Carroll, C., Hartikainen, A., & Osvaldo, M. 2019, Journal of Open Source Software, doi: [10.21105/joss.01143](https://doi.org/10.21105/joss.01143)
- Naab, R., Ganster, E., & Zhang, Z. 2023, Measurement of the astrophysical diffuse neutrino flux in a combined fit of IceCube’s high energy neutrino data. <https://arxiv.org/abs/2308.00191>
- Padovani, P., Boccardi, B., Falomo, R., & Giommi, P. 2022, MNRAS, 511, 4697, doi: [10.1093/mnras/stac376](https://doi.org/10.1093/mnras/stac376)
- Picone, J. M., Hedin, A. E., Drob, D. P., & Aikin, A. C. 2002, Journal of Geophysical Research: Space Physics, 107, SIA 15, doi: [10.1029/2002ja009430](https://doi.org/10.1029/2002ja009430)
- Plavin, A. V., Kovalev, Y. Y., Kovalev, Y. A., & Troitsky, S. V. 2023, Monthly Notices of the Royal Astronomical Society, 523, 1799, doi: [10.1093/mnras/stad1467](https://doi.org/10.1093/mnras/stad1467)

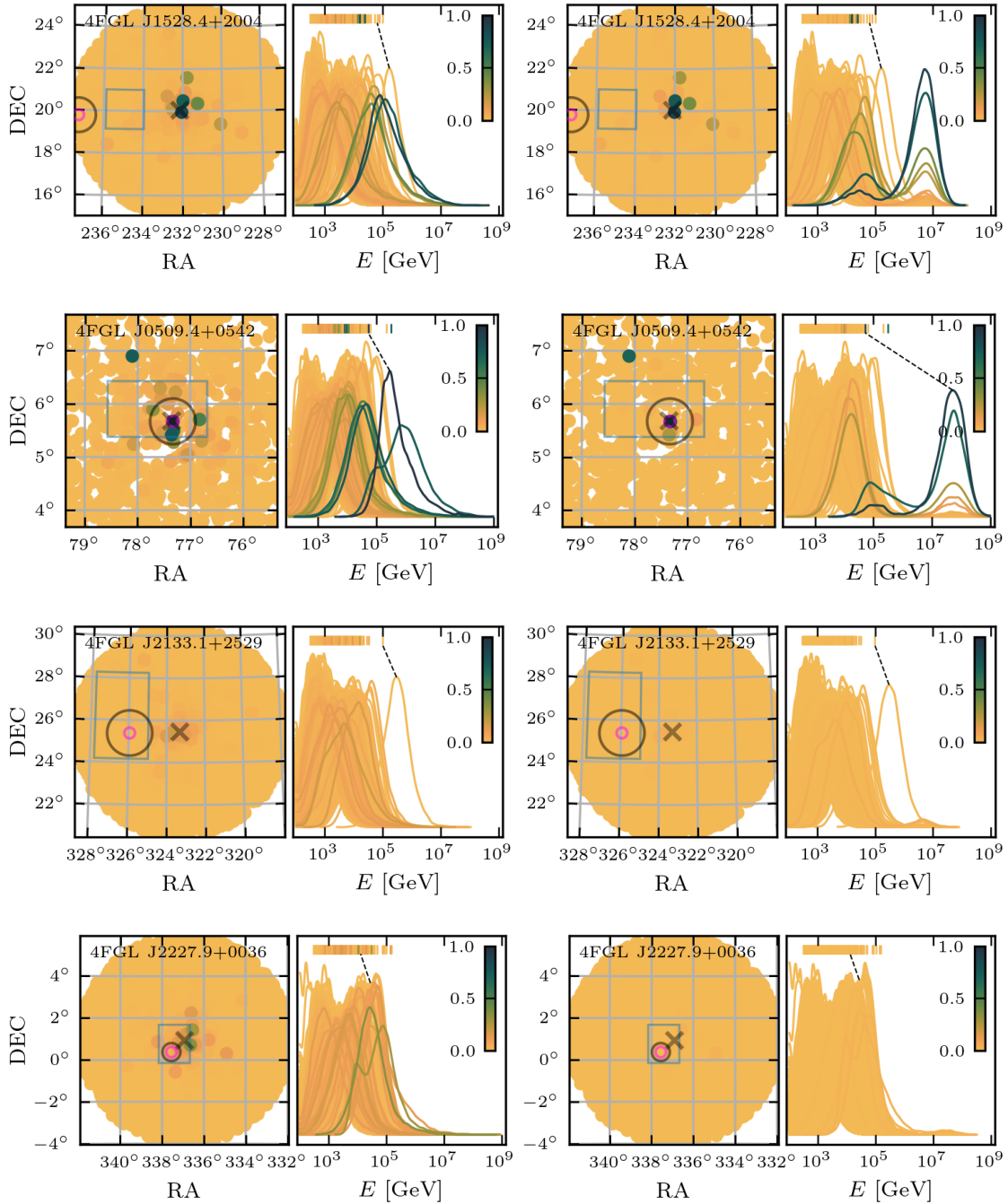


Figure A2. Comparison of power-law fits (left double column) to Fit #2 (right double column). See Fig. A1 for details.

Riehn, F., Dembinski, H., Engel, R., et al. 2017,

in ICRC 2017, Proceedings of 35th

International Cosmic Ray Conference —

PoS(ICRC2017), 301, doi: [10.22323/1.301.0301](https://doi.org/10.22323/1.301.0301)

Rodrigues, X., Karl, M., Padovani, P., et al.

2024a, The Spectra of IceCube Neutrino (SIN) candidate sources – V. Modeling and interpretation of multiwavelength and neutrino data. <https://arxiv.org/abs/2406.06667>

Rodrigues, X., Paliya, V. S., Garrappa, S., et al.

2024b, *Astronomy & Astrophysics*, 681, A119, doi: [10.1051/0004-6361/202347540](https://doi.org/10.1051/0004-6361/202347540)

- Stan Development Team. 2025, Stan Modeling Language Users Guide and Reference Manual. <http://mc-stan.org/>
- Streit, R. L. 2010, Poisson Point Processes: Imaging, Tracking, and Sensing, 1st edn. (Springer New York, NY), doi: [10.1007/978-1-4419-6923-1](https://doi.org/10.1007/978-1-4419-6923-1)
- Virtanen, P., Gommers, R., Oliphant, T. E., et al. 2020, Nature Methods, 17, 261, doi: [10.1038/s41592-019-0686-2](https://doi.org/10.1038/s41592-019-0686-2)
- Waskom, M. L. 2021, Journal of Open Source Software, 6, 3021, doi: [10.21105/joss.03021](https://doi.org/10.21105/joss.03021)
- Wenger, M., Ochsenbein, F., Egret, D., et al. 2000, A&AS, 143, 9, doi: [10.1051/aas:2000332](https://doi.org/10.1051/aas:2000332)
- Wolf, M. 2019, in International Cosmic Ray Conference, Vol. 36, 36th International Cosmic Ray Conference (ICRC2019), 1035, doi: [10.22323/1.358.01035](https://doi.org/10.22323/1.358.01035)